Journal of Harbin Engineering University
ISSN: 1006-7043

Vol 44 No. 10
October 2023

Synthesis and Characterization of SnO2/ZnO nano composites doped Some Selected Conducting Polymers for Sensing Application

[1]Ms. Swagat Sadashiv Ebhad
[1]PHD Student, Dr. APJ Abdul Kalam University,Indore,MP, India.
Department of Physics
Swagatebhad1@gmail.com

[2]Dr. Mohan N Giriya
[2]Principal, Chintamani College of Arts and Science, Gondpipri, Dist: Chandrpur, M.S, India
mohangiriya@gmail.com

ABSTRACT
The proportion of SnO_2 resulted in a reduction in light transmission and an increase in the amount of energy that was lost.
The synthesis, self-assembly, and properties of ZnO nanostructures and nanocomposites were the subjects of this research. Zinc oxide nanoparticles' production, characterization, and applications are covered in detail throughout the chapters. The following is the order of this chapter: In the first part of this paper, an investigation is conducted into asymmetric ZnO nanostructures that contain an inner cavity. The freshly produced inner space can be found in the upper section of the nanostructures, which demonstrates the anisotropy of the structure. This is in contrast to the nanostructures, which have hollow interiors. During the manufacture of ZnO asymmetric nanostructures, surfactants may regulate the self-assembly of fundamental nano-crystallites and the growth of two or more crystal planes. As was mentioned.
The nanostructures of ZnO in the shape of an hourglass were produced using hydrothermal processing. Scientists were able to figure out the specific structure of ZnO subunits as well as the mechanism behind their own self-assembly by using Tween-85. The van der Waals interactions between the surface-anchored alkylated oleate groups of the subunits are what drive the hourglass structures to assemble themselves in a linear fashion. This discovery was made possible through surface-anchored van der Waals contact. During the process of disassembling the hourglass structures, this was discovered.

Keywords*: *Synthesis, Zinc Oxide, Nanostructure, Nanocomposites, Material Properties

Introduction

Sol gel synthesis was used to synthesize ZnO and SnO_2 nano-composites and evaluate their structural, morphological, and electrochemical properties. Composite composition determines particle size and strain by X-rays. AFM shows a mainly homogeneous and granular surface with increasing SnO_2.
Photoluminescence was employed in optics. Doped samples peak-shifted slightly less than un-doped samples. Doping the host matrix and altering nano-composites' band gap energies triggered the shifting.
The SILAR method synthesizes SnO_2–ZnO nanocomposite at room temperature. XRD patterns of annealed films show SnO_2-ZnO nanocomposite formation. SEM displays SnO_2–ZnO nanocomposite's porous nanoparticle network. ZnO is cauliflower-shaped, SnO2 nanoparticle-like. Composite film elements are verified by EDS. LPG, ethanol, hydrogen sulphide, and ammonia were detected by SnO_2–ZnO nano-composite sensors.
When the ratio of SnO2 was increased, light communication decreased and energy loss rose. This was because the ratio reduced energy loss.
This work focused on ZnO-related nanostructures and nanocomposites' production, self-assembly, and properties. This doctoral thesis was compulsory reading and writing. The nine chapters of this thesis describe zinc oxide nanoparticle

creation, characterization, and application methodically. The chapters are ordered as follows: The chapters are presented in this order: Asymmetric ZnO nanostructures with cavities are examined in the first half of this article. The newly generated internal space is in the upper section of nanostructures, which has a novel structural anisotropy. This discovery was made possible by nanotube-based nanostructures. This is unlike the conventional nanostructure with a hollow center. A surfactant may regulate the self-assembly of fundamental nano-crystallites and the growth of two or more crystal planes during ZnO asymmetric nanostructure creation. Based on the concept that surfactants influence fundamental nano-crystallites' self-assembly. This proposal has been considered.

Hydrothermal method made hourglass-shaped ZnO nanostructures. This assembly succeeded. Researchers discovered ZnO subunits' unique structure and self-assembly using Tween-85. Van der Waals contact of surface-anchored alkylated oleate groups causes hour-glass structures to assemble linearly. Hour-glass structures are linearly assembled via van der Waals contact. This phenomenon was identified because van der Waals interactions are surface-anchored. This was discovered when the hourglass-shaped buildings collapsed.

Material Science and Engineering's ability to create new materials has transformed society. Thin film technology powers cutting-edge gadgets. Thin film science and technology are crucial to high-tech. Grove found that sputtering cathode with high-energy positive ions formed metal sheets. Many real-world problems require two-dimensional thin films. They fulfil the same surface functions as bulk materials but cost less. The nature, functionality, and new properties of thin films have been used to create new technologies. Thin film technology is growing daily as new technologies shrink to atoms and achieve tolerances only an electron microscope can read. Films are homogenous solids between two planes and extended in two dimensions, but limited in a third direction perpendicular to XY.

This creates modest localized warmth. When developing metal coating methods for thin plastic products, substrates often melt during first deposition cycles. Coating temperature-sensitive substrates requires monitoring source-to-substrate distances and deposition rates. Induction, electric resistance, and electron beam heating vaporize charges. Thermal, cathodic arc, and laser ablation deposit tiny layers. The laser beam penetrates a window to focus on evaporated powder from outside the evaporation system trifacial nano-control makes nanocomposites. The goal is molecular interface, structure, and morphology control. Chemical/physical qualities and functions may be unattainable separately. Nanocomposite domain sizes, topologies, and assembly must be optimized.

Solution solidifies using sol–gel. Sol-gel uses inorganic (chlorides, nitrates, sulphide) and metal organic precursors. Alkoxide precursor technique is flexible. Hydration and condensation cross-link molecular precursors. Zinc oxide, titania, and indium oxide develop at moderate temperatures.

Review of Paper

Recent Developments on I and II Series Transition Elements Doped SnO2 Nanoparticles and its Applications for Water Remediation Process: A Review Manmeet Kaur, Dixit Prasher, Ranjana Sharma, J. Water Environ. Nanotechnology, 2022

Water purifier SnO2. Dopants boost photocatalysis. Hydrothermal, sol-gel, and co-precipitation doped SnO2 nanoparticles. Select sol-homogeneity gels. TM doping boosts photocatalysis and reduces recombination. Changing pH, dopant concentration, duration, and temperature forms visible light photocatalysts. Doping kills photocatalysts. Photodegradation removed colors, medicines, and contaminants. Doped SnO2 doesn't. Water is cleaned by Nano-SnO2/UV/visible light. Nano-SnO2 removes dyes/toxicity. Irradiation source, manufacturing method, and pollutant removal were compared for photodegradation.

Water contaminants are minimized by SnO2 nanoparticles. Doping SnO2. This is for doping researchers.

SILAR synthesis of SnO2–ZnO nanocomposite sensor for selective ethanol gas K S Pakhare, B M Sargar, S S Potdar, U M Patil and R D Mane, Indian Academy of Sciences, 2022

SILAR synthesizes room-temperature SnO2–ZnO. XRD suggests SnO2–ZnO nanocomposites. SEM shows SnO2–ZnO's porous nanoparticle network. SnO2 nanoparticles, ZnO cauliflower-shaped. EDS certifies films. SnO2–ZnO nanocomposites detected LPG, ethanol, hydrogen sulfide, and ammonia. At 275°C and 24 ppm, ethanol is 56.93% sensitive. Faster composite sensors. Composite sensors benefit from intergrain heterojunctions. SnO2–ZnO sensor is ethanol-selective at low concentrations.

SILAR created SnO2–ZnO. Composite XRD exhibited rutile and wurtzite peaks. Micrographs of SnO2–ZnO nanocomposite show nanoparticle growth. SnO2 is nanoparticle-like while ZnO is cauliflower-like. TEM shows 4-20 nm crystallites. EDS-related. TC1-TC3 bandgap energy turns blue. TC3 attacks 24 ppm ethanol at 275°C. 40 seconds of ethanol activation. LPG, ammonia, and H2S are disliked by TC3. Sample TC3's SnO2–ZnO electrodes detect ethanol vapors.

ZnO: SnO2 nanocomposite efficacy for gas sensing and microbial applications Nagamalli Arasavalli, Daisy Rani Alli, BK Babu, Gurrala Ravichandra & K Sai Moshing, Indian Journal of Biochemistry & Biophysics 2022

As-synthesized Sol-gel heterogeneous co-precipitation ZnO: SnO_2 VOC sensor (SG). Selectivity is 162.69 Vacant oxygen increases conductivity. Composite ZnO/SnO2 Nanocluster sensor had best ethanol reactivity, good stability, maximum 13 A sensor current, strong selectivity, and quick repetition rate.

Structural, Optical and Microscopy Analysis of ZnO-CuO Nanocomposite Thin Films, K. Kavitha, T. Ranjeth Kumar Reddy, T. SubbaRao, R. Padmasuvarna, V. S. Vani, Adalya Journal, 2019

The nanofilms were ZnO-CuO. X-ray structure analysis (XRD). Spectrophotometers measure UV-visible and infrared light (FTIR). SEM-EDX studied surface morphology. XRD reveals crystals. 0.025 M, 0.05 M, and 0.075 M had a 3.5 eV UV-visible band gap. Calculated CuO and ZnO functional groups. SEM-EDX detected surface Zn, Cu, and O.

Variable-molarity 500°C-dipped ZnO-CuO nanocomposites. Nanocomposite crystallinity and size were measured by XRD. Peaks had hexagonal ZnO and monoclinic CuO nanocomposites. 3.5, 3.3, and 3.1 eV band gaps in ZnO-CuO thin films. SEM confirmed XRD's size and form. EDX found that zinc and cupric acetate made excellent nanocomposites.

Synthesis and structural properties of Mn-doped ZnO/Graphene nanocomposite Mahnaz Mohammadi, Afshin Maleki, Shiva Zandi, Ebrahim Mohammadi, Esmail Ghahramani, J Adv. Environ Health Res, 2018

ZnO is a photocatalytic semiconductor. Weak dispersion, aggregation, and energy gap. Dope MOS. Mn aids. Graphene improves ZnO's photocatalysis. ZnO/graphene nanocomposite transport electrons. Manganese-doped graphene/ZnO nanocomposites were developed. SEM, XRD, FTIR, AFM, DLS, and zeta potential were used. 3467 cm-1 indicates zinc in graphene, while 439 cm-1 indicates Mn. AFM measures graphene at 1.48 nm. Graphene reduced GO-ZnO-diameter. Mn's Mn and ZnO dope graphene, says the report.

Graphene/ZnO doped by Mn was synthesized by solvothermal method and studied by XRD, SEM, FTIR, AFM, and DLS.

Transparent graphene was exposed to single layer and low-layer sheets, and nanoscale Mn-ZnO particles were put on the graphene plate structure. FTIR verified the presence of Zn and Mn on graphene.

Doping was successful, and this nanocomposite might be used in photocatalytic pollutant breakdown.

Goals of thesis

The ratio of SnO_2 decreased light transmission and increased energy loss. Synthesis, self-assembly, and characteristics of ZnO nanostructures and nanocomposites were studied. Chapters explain the creation, characterization, and usage of zinc oxide nanoparticles. This chapter's order is: This article's first half investigates asymmetric ZnO nanostructures with an inner cavity. The newly generated inner space is in the nanostructures' upper area, demonstrating structural anisotropy. This differs from nanostructures' hollow interiors. Surfactants may regulate the self-assembly of fundamental nano-crystallites and the growth of two or more crystal planes during the production of ZnO asymmetric nanostructures. As suggested.

Hydrothermal processing was used to create hourglass-shaped ZnO nanostructures. Using Tween-85, scientists were able to determine ZnO subunits' unique structure and self-assembly mechanism. The linear assembly of hour-glass structures is caused by van der Waals interactions between subunits' surface-anchored alkylated oleate groups. Surface-anchored van der Waals interaction enabled this discovery. This was found when the hourglass structures were disassembled.

Aim of the Project

This thesis generates nanoparticles, accurately characterizes nanomaterial growth, and investigates nanomaterial applications. To characterize zinc oxide, a widely studied material; ZnO has great potential in UV lasers, solar cells, and field-emission electrodes. Numerous ZnO nanostructures, including pyramids, spheres, self-assemble, and nanocomposites, have been made utilizing a hydrothermal technique. This study seeks. A lot of study has been done to find synthetic conditions, including permeability and strong catalytic characteristics. UV-visible spectroscopy determines transmittance, absorbance, optical absorption coefficient, optical band gap, refractive index, dielectric constants, and other characteristics.

Tin oxide nanoparticle synthesis

SnO_2 nanoparticles were precipitated from anhydrous SnCl4 and ammonia solution. Typically, 10 mL anhydrous $SnCl_4$ was dissolved in 90 mL deionized water and magnetically agitated for 15 min. Drops of 25% aqueous ammonia were introduced to the SnCl4 solution under magnetic stirring. Ammonia solution produced a white precipitate.

The suspension was stirred overnight. Next, the Sn $(OH)_2$ precipitate was phase separated by centrifugation at 5,800 rpm and rinsed with distilled water until no chloride ion was identified. An oven at 110°C dried the wet powder overnight, followed by calcination in a muffle furnace at 400°C for 2 h. The calcined SnO2 powder was crushed with agate mortar–pestle for additional experiments.

CuO and ZnO catalysts are of interest to scientists and industry for their low temperature–low pressure methanol synthesis. Before usage, these catalysts are activated in diluted hydrogen. Copper oxide kinds are transformed into Cu metal throughout this procedure. The degree of reduction and the temperature at which it occurs depend on the CuO-ZnO particle interaction. ZnO may also alter copper reactivity in reduced catalysts in several ways. Oxide particle homogeneity and interspersion affect all of these effects.

In reality, catalyst oxide homogeneity and interspersion affect catalytic activity. TPR (Temperature-Programmed Reduction) showed how CuO-ZnO catalysts interact when oxidized or reduced. Coprecipitation at constant pH produced hydroxycarbonates precursors. This method produced well-dispersed CuO-ZnO mixed oxides, which were used to make catalysts with large surface areas and crystallite sizes below 100. The catalysts were made by thermally breaking down hydroxycarbonates precursors at 623 K in air.

The H_2 TPR study showed that CuO and ZnO interacted strongly. The connection becomes more apparent when copper content drops. In the catalyst with a lower copper loading (Cu: Zn=10:90 and 5:95 as an atomic ratio), some very small CuO-like particles interact so strongly with ZnO that they are reduced at temperatures below 50 K compared to the other catalysts.

Because CuO-like particles are likely nanostructured, this is likely. Another important discovery is that CO_2 at 573 K for 0.33 hours can partially re-oxidize copper metal in reduced catalysts to produce very tiny and even more nanostructured CuO-like species that are extremely reactive, much more so than fresh catalysts.

By using combustion as the primary mode of manufacture, a novel photocatalyst with Ag integrated Li doped ZnO nanocomposites was created. This photocatalyst was successful in reducing carbon monoxide emissions. This photo catalyst may be able to treat Candiasis and Cryptococcus, two potentially fatal skin fungal illnesses caused by fungi. Candiasis is more common.

Antibacterial activity against Candida albicans and Cryptococcus neoformans was significantly enhanced as a result of the incorporation of Li and Ag into ZnO Matrices.

The microbiological count of both fungi fell not only with the passage of time (up to 10 hours), but it also reduced in connection to the increase in the concentration of silver. This was the case even though both fungi were exposed to the same amount of silver. Following a break of two hours, the total number of bacteria dropped to 200, and then it continued to drop until it reached 100.

The clustering appears to have an easier release of silver atoms in ZnO nanocomposites with the maximum concentration of silver (5 mM), which causes a more significant decline in the population of both types of microorganisms. Despite the fact that Ag inclusion and Li doping have given the antibacterial activity a synergic impact against both of the microorganisms, this is the result.

Synthesis of ZnO photo electrode

As detailed in our previous papers, ZnO nanorods (NRs) were grown on a clean conductive substrate such Au-coated glass or florin tin oxide (FTO) using the following steps:

- The substrates were washed with acetone, isopropanol, and DI water, then ultrasonically for 10 min.
- Preparing seed solution: 0.03 M potassium hydroxide (KOH) was dissolved in 125 ml methanol and added dropwise to 0.01 M Zn $(CH_3COO)_2(2H_2O)$ in 65 methanol. A hot plate at 60 °C magnetically swirled the mixture for 2 hours at 750 rpm. Turning off the heating, the seed solution was magnetically stirred overnight.
- The seed solution was spun coated on the substrate three times at 3000 rpm for 25 s to cover the substrate with ZnO NPs for condense growth. To connect the seeds, the substrates were annealed at 120°C for 10 min.
- Equal molecular quantities (0.05 M) of zinc nitrate hex hydrate (Zn $(NO_3)2.6H_2O$) and hexamethylenetetramine (HMT) in 100 ml DI water were used to prepare the growth precursor solution. Step 3 seeded substrates were placed in Teflon samples holders and dipped horizontally in the precursor solution. The samples were placed in a 90 °C oven for 5 hours. After cooling to room temperature, DI water washed and blowing nitrogen dried the samples.

Structural analysis

The XRD patterns of the ZnO-SnO2 nanocomposites on the glass and porous silicon are presented in figure1. It is evident that the structure is polycrystalline. This structure has many peaks of hexagonal ZnO (JCPDS no. 13-0311) and many phases of tetragonal SnO2 which are Sn2O3 and Sn3O4 (JCPDS no.29-1484).

The interaction of gases with the surface depends on particle size and surface roughness. AFM images of ZS3 and ZS5 films on glass substrates are

showing in Figure which have a high homogeneous and regular granular distribution.
The average grain size these films are 63.23 nm and 108nm respectively and have RMS of 1.01nm for ZS3 and 1.28nm for ZS5. Also, they have average roughness of 0.852nm and 1.1nm respectively. The increase in the grain size with increasing of the mixed ratio may be related to the forming of compound structure as well as composite structure. The deposition of metal oxide on porous silicon improves the properties of the sensor by increasing oxygen adsorption. Figure Shows AFM images of the ZS3 and ZS5 films on porous silicon which gives the average grain size of 70.57nm and 85.53nm respectively. While the RMS and average roughness were decreased compared with thin films deposited on glass substrate

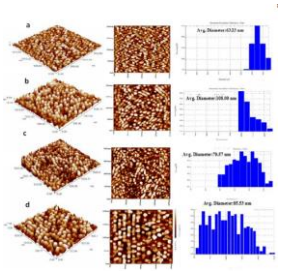

Figure: AFM images of mixed ZnO- SnO2 thin films (a): ZS3/glass (b): ZS5/glass (c): ZS3/PS (d): ZS5/PS

Synthesis of the ZnO NPs

The hydrothermal, sol-gel, solvo-thermal, and co-precipitation procedures are only some of the many ways that ZnO nanoparticles can be synthesized [38, 39]. ZnO nanoparticles can be used for the degradation of organic colors. The synthesis of varied ZnO NPs sizes and shapes can be achieved by employing a variety of growth methodologies and adjusting the associated growth parameters.
The co-precipitation technique is the most advantageous of these approaches since it is straightforward and needs only a source of zinc and a precipitating agent to be successful. Then, various factors including the precursor concentration, duration of development, and temperature may be employed in order to produce ZnO NPs with a variety of shapes and sizes. There are a variety of approaches to the synthesis of ZnO NPs, each using distinct temperatures and precursors.

NPs of magnesium doped ZnO

It is required to synthesise efficient photocatalysts under solar light in order to make more effective use of photocatalysis. This will allow for more effective utilization of the photocatalysis process. Certain elements, such as (Mg, Cd, Co, and Mn), can be utilized as a dopant to boost the photocatalysis activities of the ZnO when it is illuminated by solar light.

Among these elements, magnesium (Mg) is desirable for doping ZnO since its ionic radius is comparable to that of Zn's (0.57 and 0.60 for Mg and Zn respectively). As a result, there is a high possibility that Mg_{2+} will be incorporated into the ZnO crystal lattice. This inclusion will adjust the band gap of the ZnO, which will result in an increase in the absorption of light and a subsequent improvement in the photocatalytic effectiveness of organic dyes. Additionally, the introduction of Mg_2+ into ZnO will result in enhanced textural features as well as effective separation of electron-hole pairs, both of which would enhance the solar-driven photocatalytic efficiency.

Synthesis of Mg-doped ZnO NPs

A diluted solution of magnesium nitrate hexa-hydrate Mg $(NO_3)_2$ $6H_2O$ with varied atomic concentrations relative to Zn (0, 3, 5, and 7%) were created for the synthesis of Mg-doped ZnO NPs. This solution was then mixed with 0.2 M of NaOH solution and stirred overnight at room temperature. The final product was Mg-doped ZnO NPs. After that, 0.1 M of the solution that was made from Zn $(CH_3COO)_2$ and H_2O was added to the previous combination, and it was agitated at 750 rpm for 2 hours while being held at a temperature of 60 degrees Celsius on a hot plate.

The precipitated product was then separated by centrifugation at 4500 rpm for 2 minutes, after which it was washed several times with DI water and once with acetone. Finally, the product was dried at room temperature. In order to obtain Mg-doped ZnO NPs with varying doping concentrations (0%, 3%, 5%, and 7%), the precipitate product was dried in an oven that had been preheated to 75 degrees Celsius for six hours.

Graphene-based ZnO

Graphene (GR) is a two-dimensional material, and its carbon atoms are arranged in a honeycomb lattice structure, as illustrated in Figure. This structure is generated by a sp2 hybridized atomic orbital, which consists of sigma bonds between carbon atoms and pi ponds that are out of the plane.

GR possesses many interesting electronic properties, such as high charge carrier mobility up to 106 cm^2V-1s-1 with low resistivity (0.1-6 K/), relatively very large surface area to volume ratio, and high optical transparency over a very large spectral range from IR to UV, which makes it an excellent candidate for enhancing the performance of photocatalysts due to the improved separation efficiency of photo generated electron-hole pairs during the photo catalyst reaction. Additionally, GR possesses. During the photocatalytic process, the ZnO/GR nanocomposite is particularly noteworthy due to its capacity to block the recombination of photo generated charge carriers. This is an important step in the process. It is important to note that the wonderful capabilities of honeycomb carbon structures are not actually anything new; rather, they are abundant and naturally occurring in the form of graphite, which has been utilized in the form of minerals for quite some time.

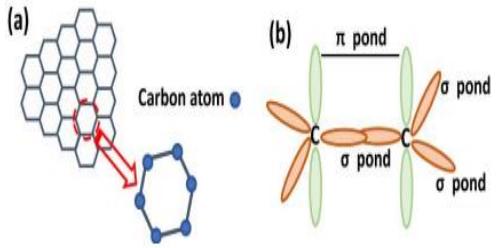

Figure: Graphene lattice structure, (b) SP2 hybridized orbitals of carbon atom

Synthesis of the ZnO/GR

According to our previously published work, the ZnO/GR nanocomposite was manufactured by dispersing GR powder at a concentration of 10 $mg.^{-1}$ into a Zn $(CH3COO)_2$ $2H_2O$ solution at a concentration of 0.01 M.

After that, a solution of potassium hydroxide (KOH) with a concentration of 0.05 M was added drop by drop while the mixture was being held in an ultrasonic water bath at a temperature of 60 degrees Celsius for ten minutes. After that, the product that had precipitated was separated by centrifuging it at a speed of 3000 rpm for ten minutes.

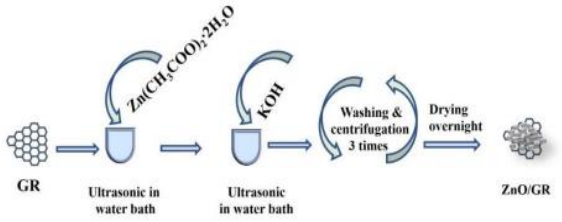

Figure: The preparation process of ZnO/GR nanocomposite

After that, the precipitate was processed further by being washed three times in DI water and acetone. After drying the precipitate in an oven warmed to 120 degrees Fahrenheit for an entire night, the ZnO/GR nanocomposite could be obtained. The method of creating the ZnO/GR nanocomposite for use in preparation

Silver-based ZnO Materials

Ag compounds are promising photocatalytic co-catalysts. Metallic silver's surface plasmon resonance (SPR) effect improves photocatalytic efficacy when deposited on ZnO [60]. The SPR, a collective oscillation of electrons caused by the electromagnetic field of incident visible light, enhances photocatalysis and depends on the size and shape of the plasmon particles.

SPRs confine or scatter light into the photo catalyst, increasing catalyst absorption. The SPR absorbs visible light at higher wavelengths, extending its absorption range. Photo catalyst electronic and photocatalytic properties will improve. This thesis examined photocatalysis performance of Ag-based semiconductors AgI, Ag2CrO4, Ag2WO4, and AgBr. Ag-compound semiconductors nanocomposite with ZnO to produce new hetero-structure with effectively enhanced photocatalysis performance

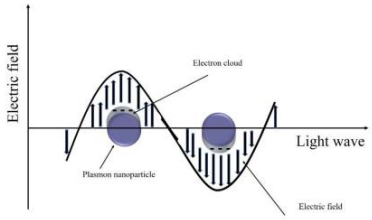

Figure: Illustration of the surface plasmon resonance in plasmon nanoparticles

Synthesis of ZnO/GR/Ag/AgI

Our previous study used varied AgI percentages to synthesise ZnO/GR/Ag/AgI nanocomposites by dispersing the as-prepared ZnO/GR in 200 ml of DI water under ultrasonic irradiation for 10 minutes. The mixer was stirred for 30 minutes with AgNO3 powder.

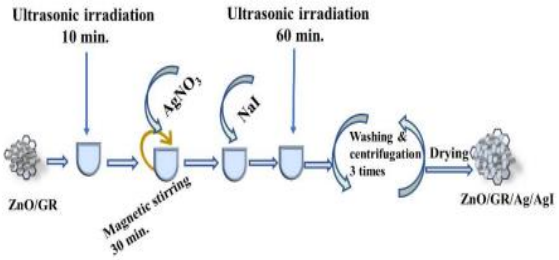

Figure: The preparation process of ZnO/GR/Ag/AgI nanocomposite

After that, NaI was dissolved in DI water at 10%, 20%, and 30% and added drop wise to the aforesaid mixture and ultrasonically irradiated for one hour. To remove salt, the product was centrifuged and rinsed twice with DI water and once with acetone. ZnO/GR/Ag/AgI nanocomposites were obtained by drying the product in a preheated oven at 75 °C for 6 hours. Figure shows the ZnO/GR/Ag/AgI nanocomposites production. The photo reduction reaction can introduce Ag particles into the nanocomposite during sample preparation or during visible solar light irradiation.

The Characterization of Structures

The use of thin films, superior growth, and patterning on a scale that is sub-micro-meter is becoming increasingly important in a variety of study areas and applications throughout the scientific and engineering disciplines. A thorough and in-depth characterization of the structure of such nanostructures is required in order to acquire an understanding of the structural characteristics of the structures. Through the use of XRD techniques, we are able to investigate the internal structure of the layers as well as the quality of the interfaces that exist between the various materials that make up a multilayer. The most definitive structural information can be obtained using XRD.

X-ray Diffraction

There is a series of non-destructive analytical techniques known as x-ray scattering techniques. These techniques provide information on the crystallographic structure, chemical composition, and physical properties of materials and thin films. These techniques are based on detecting the scattered intensity of an X-ray beam after it has impacted a sample as a function of the incident and scattered angle, polarization, and wavelength or as a function of the incident and scattered angle.

X-ray diffraction, also known as XRD, is a relatively quick analytical method that is largely utilized for the phase determination of crystalline materials. Additionally, it can provide information 53 on the size of unit cells. After being finely milled and homogenized, the material being analyzed is then

having its average bulk composition estimated. The X-ray diffraction technique has primarily been utilized in two different applications: the first of which is to determine the structure of crystalline materials, and the second is to characterize the fingerprint of crystalline substances.

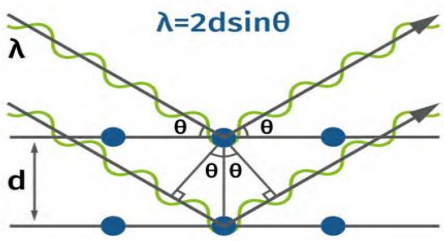

Figure: Reflection of X-rays from two planes of atoms in a solid

The easy crystalline solid has its own distinctive characteristic X-ray powder pattern, which can be utilized as a "fingerprint" for the purpose of identifying the substance. After the material has been identified, X–ray crystallography can be used to figure out its structure. This involves figuring out how the atoms pack together in the crystalline state, as well as the inter–atomic distance and angle, among other things.
X-ray diffraction is the method that makes it easiest to determine the dimensions and configuration of the unit cell of any chemical. Electromagnetic waves with a wavelength of around 1 angstrom are known as x-rays. When X-rays strike the surface of a crystal, the rays are reflected from the crystal in the form of a figure.

The reflection obeys the following Bragg's law,

$$2\square\square\square\square\theta = \square\square$$

Were
d is the distance between crystal planes,
θ is the incident angle of X-ray,
λ is the wavelength of the X–ray and
n is a positive integer.

Bragg's law also suggests that the diffraction is only possible when λ <2d

Surface thickness in thin films are about 3000 Å, can be investigated using XRD. Thicker films can be characterized by reflection high-energy electron diffraction (RHEED). Analysis of the diffraction patterns obtained by these techniques and composition with standard ASTM data can reveal the existence of different crystallographic phases in the film, their relative abundance, the lattice parameters and any preferred orientations.
Using' values the set of lattice planes (h k l) are identified from the standard data and the lattice parameters are calculated using the relations. For hexagonal crystal structure the lattice parameters can be determined using the relation,

$$\frac{1}{d^2} = \left[\frac{4}{3}\left(\frac{h^2+hk+k^2}{a^2}\right) + \frac{l^2}{c^2}\right]^{\frac{1}{2}}$$

The lattice constants a and c for tetragonal crystal structure are determined from the Equation

$$\frac{1}{d^2} = \left(\frac{h^2+k^2}{a^2}\right) + \frac{L^2}{c^2}$$

Were,
h, k and l are the indices of the crystal planes,
d is the interplanar spacing and
β is the full-width half maximum.

Crystallite size (D) is the of the effective crystal domain. It contributes to the peak broadening and as crystallite size decreases, the full width increases. The average D of the film is determined by using Debye Scherrer formula

$$D = \frac{K\lambda}{\beta \cos\theta}$$

Were

k is a constant known as shape factor and taken as 0.94,
λ is the wavelength of X-rays.
The origin of micro strain (ε) is calculated using the relation

$$\varepsilon = \frac{\beta\cos\theta}{4}$$

The dislocation density (δ) is the dislocation lines per unit area of the crystal, can also be evaluated from the crystalline size 'D' using the formula

$$\delta = \frac{1}{D^2}$$

Polymers Used to Sensing Application

Natural Rubber

Rubber, also known as India rubber, latex, Amazonian rubber, caucho, or caoutchouc, is made up of polymers of the organic compound isoprene, with trace amounts of other organic compounds present as impurities. Other names for rubber include India rubber, latex, caucho, or caoutchouc. Elastomers are a category that includes the varieties of **polyisoprene** that are utilized as natural rubbers.

Figure: Pieces of natural vulcanized rubber

Latex from the rubber tree (Hevea Brasiliense's) or other plants is the most common type of rubber that is extracted during harvesting at this time. "Tapping" is the technique that involves cutting incisions in the bark of the tree and collecting the fluid that is released from those incisions in capillaries. The latex is a milky, white, and sticky colloid. The raw latex is then processed further to produce a rubber product that is suitable for commercial use. In major areas, the collection cup containing the latex is left to congeal on its own.

After the coagulated mass has been recovered, it is then processed into dry forms so that it can be sold. Natural rubber finds widespread use in a diverse range of applications and products, either on its own or in conjunction with a variety of other materials. It is water resistant, has a high stretch-to-resilience ratio, and has a big stretch ratio in the majority of its practical forms.

Properties of Natural Polymer

Rubber has unique physical and chemical properties. Rubber's stress–strain behavior is generally hyperplastic due to the Mullins and Payne effects. Rubber strain crystallizes. Ozone cracking and vulcanization are possible in natural rubber due to weaker allylic C-H bonds in each repeat unit. Turpentine and naphtha are rubber solvents. Before immersion, rubber is shred since it doesn't dissolve easily. A solution of ammonia can inhibit raw latex coagulation. Rubber melts around 180 °C.

Cellulose Polymer

The chemical formula for cellulose is n, and it is a polysaccharide that consists of a linear chain of several hundred to many thousands of -linked D-glucose units. Cellulose is classified as an organic substance. The basic cell wall of green plants, many types of algae, and oomycetes all include cellulose, which is an essential component in terms of its structural function.

Cellulose dissolves in numerous media, including commercial technology. Reversible dissolution techniques produce regenerated celluloses from pulp.

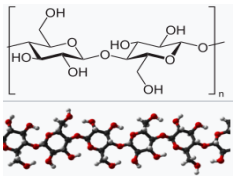

Figure: Cellulose Shell

Alkali-soluble carbon disulfide is the main solubilizer. Schweizer's reagent, N-methyl morpholine N-oxide, and dimethylacetamide lithium chloride are others. These agents usually make cellulose soluble. The agents are withdrawn

while fibres develop. Many ionic solutions dissolve cellulose.

Many goods can be made from regenerated cellulose. Regenerated cellulose was first utilized as a clothing textile, but it is now also employed to make disposable medical equipment and artificial membranes.

Properties of Cellulose

Many features of cellulose depend on its chain length or degree of polymerization, the number of glucose units per polymer molecule. Wood pulp cellulose has chain lengths between 300 to 1700 units, while cotton, other plant fibres, and bacterial cellulose contain 800 to 10,000 units. Unlike long-chain cellulose, cyclodextrins are water- and organic solvent-soluble molecules generated from cellulose breakdown.

Bacterial cellulose is clean, has a higher water content, and has higher tensile strength due to longer chain lengths than plant-derived cellulose, which is frequently mixed with hemicellulose, lignin, pectin, and other compounds.

Vinyl Chloride Polymer

Vinyl chloride is an organochloride identified by the formula $H_2C=CHCl$. Also termed vinyl chloride

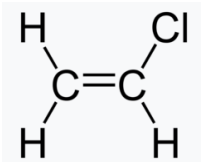

monomer or chloroethene. This colorless industrial chemical is mostly used to make poly. Vinyl chloride monomer is one of the twenty leading petrochemical producers.

Organochloride vinyl chloride is H2C=CHCl. It is also called VCM or chloroethene. This colorless compound is an essential industrial chemical used to make poly (vinyl chloride). Vinyl chloride monomer is one of the top twenty global petrochemical producers. The US produces the most vinyl chloride due of its low chlorine and ethylene costs. One of the largest vinyl chloride consumers and manufacturers is China.

Vinyl chloride is combustible, carcinogenic, and sweet-smelling. It is generated when soil microbes break down chlorinated solvents. Vinyl chloride produced by industries or created via chlorinated chemical breakdown can infiltrate the air and water. Landfills often contain vinyl chloride.

POLIANILINE (PANI) Polymer

Polyaniline (PANI) is a conducting polymer and organic semiconductor of the semi-flexible rod polymer family. The compound has been of interest because of its electrical conductivity and mechanical properties. Polyaniline is one of the most studied conducting polymers

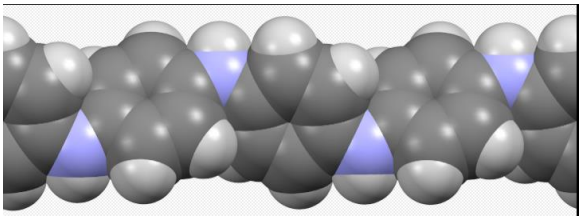

Figure: Polyaniline (PANI)

A multi-stage emeraldine base model is proposed. The reaction begins with pernigraniline PS salt oxidation. Pernigraniline is converted to emeraldine salt in the second stage as aniline monomer oxidizes to radical cation.

Depending on supplier and synthetic technique, polyaniline is manufactured as long-chain polymer aggregates, surfactant stabilized nanoparticle dispersions, or stabilizer-free nanofiber dispersions. Polyaniline dispersions stabilized by surfactants or dopants

REFERENCES

1) Morphological and Optical Properties of SnO2Doped ZnO Nanocompositesfor Electrochemical Sensing of Hydrazine, Atif Mossad Ali, Omniat Qreshah, Adel A. Ismail,Farid A. Harraz, Hamed Algarni, Mohammed A. Assiri, Mohd Faisal, Wee Siong Chiu, International Journal of Electrochemical Science, 2019

2) Microwave Assisted Synthesis, Characterization and Photo-Catalytic Study Of Cu/Zno Nanocomposite, Vaishali Prasad, G. Gnanamani Simiyon, Ansha Elizabeth Mammen and N. Jayaprakash, RJC, 2019
3) Photocatalytic Degradation Mechanism of Malachite Green Dye Using Cu2+ Doped Tin Oxide-Zinc Oxide Nanocomposites K.J.Abhirama & K.U.Madhu, 2019
4) Structural, Optical and Microscopy Analysis of ZnO-CuO Nanocomposite Thin Films, K.Kavitha, T.Ranjeth Kumar Reddy, T. SubbaRao, R.Padmasuvarna, V.S.Vani, Adalya Journal, 2019
5) Improved photocatalytic activity of Sr doped SnO2 nanoparticles: A role of oxygen vacancy Ateeq Ahmed, M. Naseem Siddique, Umair Alam, T. Ali, P. Tripathi, Applied Surface Science, elsevier, 2019
6) Preparation and characterization of zno: Sno2 nanocomposite thin films on porous silicon as H2s gas sensor ,h. S. Al-jumaili, m. N. Jasim, Journal of Ovonic Research, 2019
7) Synthesis and structural properties of Mn-doped ZnO/Graphene nanocomposite Mahnaz Mohammadi, Afshin Maleki, Shiva Zandi, Ebrahim Mohammadi, Esmail Ghahramani, J Adv. Environ Health Res, 2018
8) Study of structural and optical properties of SnO2 nanoparticles developed by sol-gel route, Vijay Garg, Harsh Sharma, Journal of Emerging Technologies and Innovative Research (JETIR), 2018
9) Surface morphological study of TiO2-doped Sno2 nanocomposites, Vineet Kumar Pandey, Prof.C.K.Dixit, 2018
10) Synthesis and characterization of Zno and Sno2 doped polyaniline nano composites, Hamjade PT, Khaire ND, Motke SG, Research article, 2018
11) Characteristics of the Bipolar Resistive Switching Behavior in Memory Device with Au/ZnO/ITO Structure Hongjun Wang , Yuanyuan Zhu , Yong Liu, Accepted Manuscript, 2018
12) Photoluminescence Study of Tin Oxide-Zinc Oxide Nanocomposites, K.J.Abhirama, K.U.Madhu, International Journal of Scientific Research in Physics and Applied Sciences, 2018
13) An overview of the synthesis of CuO-ZnO nanocomposite for environmental and other applications, Susmita Das and Vimal Chandra Srivastava, Nanotechnol Rev 2018
14) Synthesis Of NiO Doped ZnO/MWCNT Nanocomposite And Its Charecterization For Photocatalytic & Antimicrobial Applications D. Saravanakkumar, R. Karthika, S. Ganasaravanan3, S. Sivaranjani, S.Pandiarajan, B. Ravikumar, A. Ayeshamariam, IOSR Journal of Applied Physics (IOSR-JAP) 2018
15) Influence of Mg Doping on ZnO Nanoparticles for Enhanced Photocatalytic Evaluation and Antibacterial Analysis, K. Pradeev raj1,2, K. Sadaiyandi3, A. Kennedy1, Suresh Sagadevan4,6*, Zaira Zaman Chowdhury, Mohd Rafie Bin Johan, Fauziah Abdul Aziz, Rahman F. Rafique, R. Thamiz Selvi8 and R. Rathina bala, Nanoscale Research Letters, 2018
16) Met-chemically prepared low-dimensional ZnO/ Al2O3/Cr2O3 nanoparticles for xanthine sensor development using an electrochemical method M. M. Alam, Abdullah M. Asiri, M. T. Uddin, M. A. Islam and Mohammed M. Rahman, 2018
17) Synthesis and Electrical Characterization of Cu2+ doped (SnO2)1x(ZnO)x nanocomposites, K.J.Abhirama, K.U.Madhu, Int. Journal of Engineering Research and Application, 2017
18) Synthesis, Characterization and Visible Light Degradation of Organic dye by Chemically Synthesized ZnO/γ-Fe2O3 Nanocomposites Gaurav Hitkari, Sandhya Singh and Gajanan Pandey, International Journal of Advanced Research in Science, Engineering and Technology, 2017

19) Graphene oxide/SnO2 nanocomposite as sensing material for breathalyzers: Selective detection of ethanol in the presence of automotive CO and hydrocarbons emissions, M. Arvani, H. Mohammad Aliha, A.A. Khodadadia and Y. Mortazavi, Sharif University of Technology, Scientia Iranica, 2017
20) effect of calcination temperature on performance of ZnO nanoparticles for dye-sensitized solar cells, Amir Moradi Golsheikh, Khosro Zangeneh Kamali, Nay Ming Huang, Ali Khorsand Zak, ACCEPTED MANUSCRIPT, 2017
21) Optimize area proiect ării arcurilor cu for composite follows and metodologia suprafeței de răspuns optimization of composite leaf spring design using response surface methodology, S. Rajesh, G. B. Bhaskar, R.subash, K. Pazhanivel, S. Suresh sagadevan, Revista Română de Materiale / Romanian Journal of Materials 2017
22) Synthesis and Structural Investigations of ZnO–SnO2 Nanocomposite by Sol–Gel Method, V. Muthupriyal, D. Muthu Raj, E. Kumar, journal of nano-science and technology, 2017
23) Synthesis and characterization of nanostructures of ZnO and ZnO/Graphene composites for the application in hybrid solar cells, Hina Y. Abbasi, Amir Habib, Muhammad Tanveer, Journal of Alloys and Compounds, ELSEVIER, 2017
24) Structural, dielectric and optical investigation of chemically synthesized Ag-doped ZnO nanoparticles composites, Suresh Sagadevan, Kaushik Pal, Zaira Zaman Chowdhury, M. Enamul Hoque, J Sol-Gel Sci Technol, 2017
25) ZnO nanorods/graphene oxide sheets prepared by chemical bath deposition for volatile organic compounds detection, Beatriz A. Vessalli, Cecilia A. Zito, Tarcísio M. Perfecto, Diogo P. Volanti, Talita Mazon, Journal of Alloys and Compounds, elsevier, 2017